WILLIAM & MARY
CHARTERED 1693

W&M ScholarWorks

Arts & Sciences Articles

Arts and Sciences

2015

Search for baryon-number and lepton-number violating decays of Lambda hyperons using the CLAS detector at Jefferson Laboratory

M. E. McCracken

A. S. Biselli

C. A. Meyer

K. A. Griffioen
College of William and Mary

Follow this and additional works at: https://scholarworks.wm.edu/aspubs

Search for baryon-number and lepton-number violating decays of Λ hyperons using the CLAS detector at Jefferson Laboratory

M. E. McCracken,[1,2,*] M. Bellis,[3] K. P. Adhikari,[28] D. Adikaram,[28] Z. Akbar,[13,†] S. Anefalos Pereira,[17] R. A. Badui,[12] J. Ball,[9] N. A. Baltzell,[4,33,†] M. Battaglieri,[18] V. Batourine,[35,24] I. Bedlinskiy,[22] A. S. Biselli,[11,2] S. Boiarinov,[35] W. J. Briscoe,[14] W. K. Brooks,[36,35] V. D. Burkert,[35] T. Cao,[33] D. S. Carman,[35] A. Celentano,[18] S. Chandavar,[27] G. Charles,[21] L. Colaneri,[19,31] P. L. Cole,[15] M. Contalbrigo,[16] O. Cortes,[15] V. Crede,[13] A. D'Angelo,[19,31] N. Dashyan,[42] R. De Vita,[18] E. De Sanctis,[17] A. Deur,[35] C. Djalali,[33] G. E. Dodge,[28] R. Dupre,[21] A. El Alaoui,[36] L. El Fassi,[28] E. Elouadrhiri,[35] P. Eugenio,[13] P. Fedotov,[33,32] S. Fegan,[18] R. Fersch,[8] A. Filippi,[20] J. A. Fleming,[37] B. Garillon,[21] N. Gevorgyan,[42] G. P. Gilfoyle,[30] K. L. Giovanetti,[23] F. X. Girod,[35,9] E. Golovatch,[32] R. W. Gothe,[33] K. A. Griffioen,[41] M. Guidal,[21] L. Guo,[12,35] K. Hafidi,[4] H. Hakobyan,[36,42] C. Hanretty,[35] M. Hattawy,[21] K. Hicks,[27] M. Holtrop,[25] S. M. Hughes,[37] Y. Ilieva,[33,14] D. G. Ireland,[38] B. S. Ishkhanov,[32] E. L. Isupov,[32] D. Jenkins,[39] H. Jiang,[33] H. S. Jo,[21] D. Keller,[40] G. Khachatryan,[42] M. Khandaker,[15,26] A. Kim,[10] W. Kim,[24] A. Klein,[28] F. J. Klein,[7] V. Kubarovsky,[35,29] P. Lenisa,[16] K. Livingston,[38] H. Y. Lu,[33] I. J. D. MacGregor,[38] M. Mayer,[28] B. McKinnon,[38] M. D. Mestayer,[35] C. A. Meyer,[2] M. Mirazita,[17] V. Mokeev,[35,32] C. I. Moody,[4] K. Moriya,[2,‡] C. Munoz Camacho,[21] P. Nadel-Turonski,[35] L. A. Net,[33] S. Niccolai,[21] M. Osipenko,[18] A. I. Ostrovidov,[13] K. Park,[35,24,§] E. Pasyuk,[35] S. Pisano,[17] O. Pogorelko,[22] J. W. Price,[5] S. Procureur,[9] Y. Prok,[28,40] B. A. Raue,[12,35] M. Ripani,[18] A. Rizzo,[19,31] G. Rosner,[38] P. Roy,[13] F. Sabatié,[9] C. Salgado,[26] R. A. Schumacher,[2] E. Seder,[10] Y. G. Sharabian,[35] Iu. Skorodumina,[33,32] D. Sokhan,[38] N. Sparveris,[34] P. Stoler,[29] I. I. Strakovsky,[14] S. Strauch,[33,14] V. Sytnik,[36] Ye Tian,[33] M. Ungaro,[35] H. Voskanyan,[42] E. Voutier,[21] N. K. Walford,[7] D. P. Watts,[37] X. Wei,[35] M. H. Wood,[6,33] N. Zachariou,[33,‖] L. Zana,[37,25] J. Zhang,[35] Z. W. Zhao,[28,35] and I. Zonta[19,31]

(CLAS Collaboration)

[1]*Washington & Jefferson College, Washington, Pennsylvania 15301, USA*
[2]*Carnegie Mellon University, Pittsburgh, Pennsylvania 15213, USA*
[3]*Siena College, Loudonville, New York 12220, USA*
[4]*Argonne National Laboratory, Argonne, Illinois 60439, USA*
[5]*California State University, Dominguez Hills, Carson, California 90747, USA*
[6]*Canisius College, Buffalo, New York 14208, USA*
[7]*Catholic University of America, Washington, D.C., 20064, USA*
[8]*Christopher Newport University, Newport News, Virginia 23606, USA*
[9]*CEA, Centre de Saclay, Irfu/Service de Physique Nucléaire, 91191 Gif-sur-Yvette, France*
[10]*University of Connecticut, Storrs, Connecticut 06269, USA*
[11]*Fairfield University, Fairfield, Connecticut 06824, USA*
[12]*Florida International University, Miami, Florida 33199, USA*
[13]*Florida State University, Tallahassee, Florida 32306, USA*
[14]*The George Washington University, Washington, D.C., 20052, USA*
[15]*Idaho State University, Pocatello, Idaho 83209, USA*
[16]*INFN, Sezione di Ferrara, 44100 Ferrara, Italy*
[17]*INFN, Laboratori Nazionali di Frascati, 00044 Frascati, Italy*
[18]*INFN, Sezione di Genova, 16146 Genova, Italy*
[19]*INFN, Sezione di Roma Tor Vergata, 00133 Rome, Italy*
[20]*INFN, Sezione di Torino, 10125 Torino, Italy*
[21]*Institut de Physique Nucléaire, CNRS/IN2P3 and Université Paris Sud, Orsay, France*
[22]*Institute of Theoretical and Experimental Physics, Moscow, 117259, Russia*
[23]*James Madison University, Harrisonburg, Virginia 22807, USA*
[24]*Kyungpook National University, Daegu 702-701, Republic of Korea*
[25]*University of New Hampshire, Durham, New Hampshire 03824, USA*
[26]*Norfolk State University, Norfolk, Virginia 23504, USA*
[27]*Ohio University, Athens, Ohio 45701, USA*
[28]*Old Dominion University, Norfolk, Virginia 23529, USA*
[29]*Rensselaer Polytechnic Institute, Troy, New York 12180-3590, USA*
[30]*University of Richmond, Richmond, Virginia 23173, USA*
[31]*Universita' di Roma Tor Vergata, 00133 Rome, Italy*
[32]*Skobeltsyn Institute of Nuclear Physics, Lomonosov Moscow State University, 119234 Moscow, Russia*
[33]*University of South Carolina, Columbia, South Carolina 29208, USA*
[34]*Temple University, Philadelphia, Pennsylvania 19122, USA*
[35]*Thomas Jefferson National Accelerator Facility, Newport News, Virginia 23606, USA*

[36]*Universidad Técnica Federico Santa María, Casilla 110-V Valparaíso, Chile*
[37]*Edinburgh University, Edinburgh EH9 3JZ, United Kingdom*
[38]*University of Glasgow, Glasgow G12 8QQ, United Kingdom*
[39]*Virginia Tech, Blacksburg, Virginia 24061, USA*
[40]*University of Virginia, Charlottesville, Virginia 22901, USA*
[41]*College of William and Mary, Williamsburg, Virginia 23187, USA*
[42]*Yerevan Physics Institute, 375036 Yerevan, Armenia*

We present a search for ten baryon number violating decay modes of Λ hyperons using the CLAS detector at Jefferson Laboratory. Nine of these decay modes result in a single meson and single lepton in the final state ($\Lambda \to m\ell$) and conserve either the sum or the difference of baryon and lepton number ($B \pm L$). The tenth decay mode ($\Lambda \to \bar{p}\pi^+$) represents a difference in baryon number of two units and no difference in lepton number. We observe no significant signal and set upper limits on the branching fractions of these reactions in the range $(4\text{–}200) \times 10^{-7}$ at the 90% confidence level.

I. INTRODUCTION

The Standard Model (SM) of particle physics [1–3] has had great success in interpreting and predicting experimental results since its conception in the late 1960s. There are, however, features of our Universe that are inconsistent with the SM framework. Astronomical observations suggest that our Universe is dominated by matter over antimatter [4,5]. Sakharov proposed in 1967 that this asymmetry suggests fundamental interactions that violate CP symmetry and baryon number conservation [6]. The observed quark-sector CP violation, combined with baryon number violating (BNV) processes that *are* allowed by the Standard Model, are insufficient [7] to account for the observed matter-antimatter asymmetry in our Universe. A possible explanation for this discrepancy is that there are yet-unobserved interactions that violate baryon number conservation.

Baryon number violating reactions are features of several theoretical extensions to the Standard Model, perhaps most notably the $SU(5)$ Grand Unified Theory (GUT) of Georgi and Glashow [8], $SU(5)$ being the larger gauge group in which the Standard Model's $SU(3) \times SU(2)$ are embedded [9]. The $SU(5)$ theory proposes the existence of two new gauge bosons, the X and Y leptoquarks, so called because they allow vertices such as $q \to X\ell$, where q is a quark and ℓ a lepton. Other experiments have been performed to search for BNV processes in decays of the nucleon [10–12], τ leptons [13–15], top quarks [16], hadrons with bottom and charm quarks [17,18], and the Z boson [19], but no signal has

yet been observed. The most stringent limits on such processes come from nucleon decays, and these have been used to constrain BNV decays in higher-generation (i.e., c, b, and t) quarks [20]. However, multiple amplitudes can contribute to a given decay process, and these amplitudes can interfere either constructively or destructively, depending on their relative phases. The theoretical calculations that constrain these BNV processes do not take into account interference between the amplitudes due to the large parameter space. This allows for nonobservation in one mode (e.g., decays involving the u or d quark) while still being consistent with observable BNV processes in some other mode (e.g., coupling to another quark flavor).

Here we present a search for baryon number (B) and lepton number (L) nonconserving decays of the Λ hyperon as a direct probe of couplings of BNV interactions to the strange quark. By summing the branching fractions and experimental uncertainties (in quadrature) of the six observed Λ decay modes [12], we find the total branching fraction to be 1.001 ± 0.007, implying that there is room for yet-unobserved decay modes.

We investigated eight decay modes in which the Λ decays to a charged meson and a charged lepton, conserving charge in all decays. The meson is either a $\pi^{\pm}$ or $K^{\pm}$, and the lepton is either an $e^{\mp}$ or an $\mu^{\mp}$. We produced the Λ by means of a photon beam incident on a liquid hydrogen target through the exclusive reaction $\gamma p \to K^+ \Lambda$. For these eight modes, we could completely reconstruct the three final-state particles. We also searched for the decay of a Λ to a K_S^0 and a neutrino, which must be inferred from the missing momentum. Selection of these nine channels is motivated by searching for the decay of the Λ to a lighter pseudoscalar meson. In each case, the final-state lepton is included to preserve charge and angular momentum conservation. Thus, violation of L in these reactions is a consequence of B violation rather than a primary motivation.

In addition, we searched for the BNV decay of the Λ to an antiproton and a π^+, for which we can completely

---
*mmccracken@washjeff.edu
[†]Present address: Thomas Jefferson National Accelerator Facility, Newport News, VA 23606, USA.
[‡]Present address: Arizona State University, Tempe, AZ 85287, USA.
[§]Present address: Old Dominion University, Norfolk, VA 23529, USA.
[‖]Present address: Edinburgh University, Edinburgh EH9 3JZ, United Kingdom.

reconstruct the final state. The $\Lambda \to \bar{p}\pi^+$ reaction presents an opportunity to search for $\Lambda - \bar{\Lambda}$ oscillations, i.e., a process by which the Λ oscillates into its antiparticle counterpart ($\bar{\Lambda}$), which then undergoes a Standard Model decay ($\bar{\Lambda} \to \bar{p}\pi^+$). Though there is not a simple way to picture this reaction proceeding via X boson coupling, theoretical and experimental (e.g., Refs. [21,22]) work has been performed by other groups looking for similar oscillations of the neutron. Such baryon-antibaryon oscillations would have far-reaching implications and are often held up as evidence for high-energy theories ranging from seesaw models [23,24] to extra dimensions [25].

The properties of these reactions are summarized in Table I. These specific decays were chosen for several reasons:

(i) Each reaction shows evidence of $\Delta B \neq 0$ and/or $\Delta L = \pm 1$.

(ii) Each reaction conserves electric charge and angular momentum.

(iii) This selection includes reactions that either preserve or violate $B - L$, a conserved quantity proposed by several GUTs [26].

(iv) The CLAS detector is optimized to reconstruct the final-state charged particles produced in each reaction, except for the neutrino which can be inferred by calculating the missing 4-momentum in the event.

A. Analysis overview

This analysis was performed in three stages. Here, we present a brief outline; details of each stage will be given in the following sections.

Λ *identification*. To assess the sensitivity of our study, we first determined the number of Λ hyperons produced during the run period. We did so by considering the charged decay mode, $\Lambda \to p\pi^-$. We applied a set of simple cuts on kinematic observables and timing for the recoil K^+ to effectively identify potential Λ events. We used this sample to determine the total number of $\gamma p \to K^+\Lambda \to K^+ p\pi^-$ events detected and then acceptance corrected to find the total number of $\gamma p \to K^+\Lambda \to K^+ p\pi^-$ events produced during the run period.

TABLE I. Properties of conserved quantities for each Λ BNV channel. Here ℓ represents a lepton, either e or μ. The rightmost column shows the detected final-state particles for each channel. Subscripts denote recoil (r) or decay (d) kaons.

Decay	ΔB	ΔL	$\Delta(B-L)$	Detected
$\Lambda \to K^+ \ell^-$	-1	$+1$	-2	K_r^+, K_d^+, ℓ^-
$\Lambda \to K^- \ell^+$	-1	-1	0	K_r^+, K_d^-, ℓ^+
$\Lambda \to \pi^+ \ell^-$	-1	$+1$	-2	K_r^+, π^+, ℓ^-
$\Lambda \to \pi^- \ell^+$	-1	-1	0	K_r^+, π^-, ℓ^+
$\Lambda \to K_S^0 \nu, K_S^0 \bar{\nu}$	-1	± 1	$0, -2$	K_r^+, π^+, π^-
$\Lambda \to \bar{p}\pi^+$	-2	0	-2	$K_r^+, \bar{p}, \pi^+$

Channel-specific tuning. When searching for evidence of the BNV decays listed in Table I, we performed a blind search. We developed a set of background separation cuts for each BNV channel, based on timing information for all charged final-state particles and kinematic observables for the event. In developing these cuts, we balanced the optimization of kinematic cuts for both discovery and upper-limit sensitivity by maximizing a figure of merit (approximately the BNV signal efficiency divided by the square root of the number of background events). We assessed the signal efficiency using a Monte Carlo technique and the background size using sidebands of the blinded signal region. This step provided a set of cuts for each BNV channel that reduced background and provides optimal analysis power.

Unblinding. We then unblinded the signal regions of kinematic variable plots and determined whether a signal was present. For nine of the decays, the expected backgrounds were 0 or 1 event, and so we used the Feldman–Cousins method [27] to determine upper bounds on branching fractions; for the remaining channel, the backgrounds were higher, and so we scanned the relevant parameters in our fit to determine the 90% coverage for the number of signal events in the data set.

II. CLAS DETECTOR AND DATA SET

The CLAS detector is described in detail elsewhere [28]. The data set comes from the g11 run period, which collected data during May and June 2004. A bremsstrahlung photon beam was produced by a 4.023-GeV electron beam incident on a gold radiator. Electrons were provided by Continuous Electron Beam Accelerator Facility in 2-ns bunches. Photon energy and timing information were provided by a tagging spectrometer which directs the electrons after the radiator through a magnetic field and onto a set of scintillators, providing photon energy resolution of 4.0 MeV.

For this analysis, we made use of the CLAS drift chamber and toroidal magnet systems to measure the momenta of the charged final-state particles. Velocity measurements were made by a start counter (consisting of scintillators placed within 11.6 cm of the target) and a set of time-of-flight (TOF) scintillators located approximately 4 m from the target. Timing information from the photon tagger was combined with this system to calculate a velocity for each charged track, and this was compared with the particle hypothesis in the particle identification (PID) algorithm. More details of the g11 data set, calibration procedures, and systematic studies can be found in (e.g.) Ref. [29].

III. IDENTIFICATION OF $\gamma p \to K^+\Lambda \to K^+ p\pi^-$ EVENTS

To compare the branching fraction for a BNV decay mode to that of the Standard Model $\Lambda \to p\pi^-$ decay, we first had to assess the number of Standard Model decays that occurred during the data-taking period. We did so by

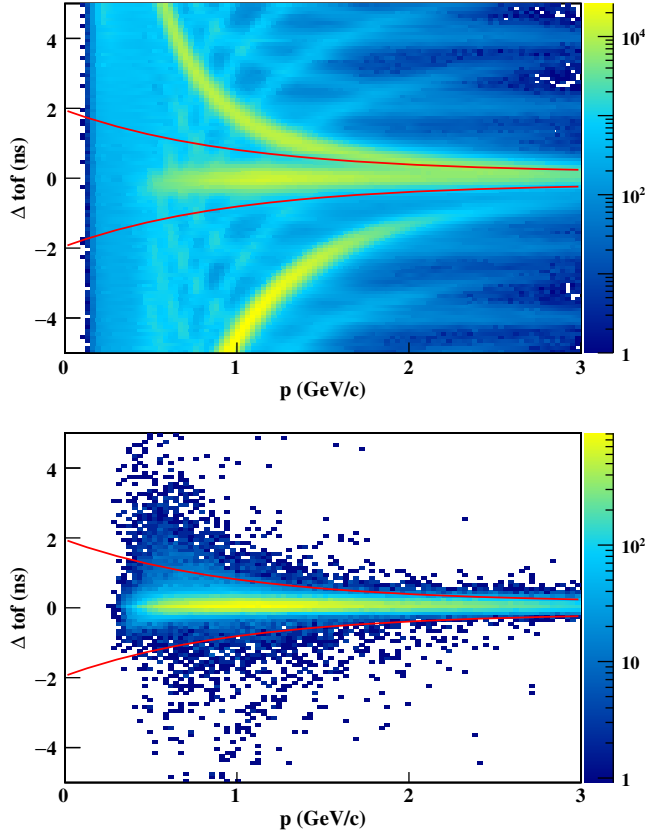FIG. 1 (color online). Δtof vs momentum (p) for K^+ candidate tracks for data (top) and MC (bottom) that pass the cut on MM^2. The red curves show the upper and lower bounds of the K^+ PID cuts. Several additional structures are apparent in data distribution. The band of events with $\Delta tof \gtrsim 1$ ns represents μ^+ from K^+ decay, that with $\Delta tof \lesssim 1$ ns represents protons, and the less populated bands represent events matched with photons from a different 2-ns beam bunch. The majority of these are removed by further cuts.

investigating the (exclusive) $\gamma p \to K^+ \Lambda \to K^+ p \pi^-$ reaction. Earlier studies [29] have shown that the $\gamma p \to K^+ \Lambda$ signal is easily separable from background when all three final-state particles are reconstructed.

Because a different set of background separation cuts was applied to the BNV channels, we corrected the number of reconstructed signal events (N_{rec}) to find N_{prod}, the number of $\gamma p \to K^+ \Lambda \to K^+ p \pi^-$ events that were produced in CLAS during the run period. To calculate the efficiency of the detector and analysis cuts, we generated 3×10^6 Monte Carlo (MC) $\gamma p \to K^+ \Lambda$ events and weighted the distribution of these events in $\cos\theta^K_{cm}$ (the K^+ production angle in the center-of-mass frame) according to published $d\sigma/d\cos\theta$ data [29]. Photon energies between 0.909 (threshold for $K^+ \Lambda$ production) and 3.860 GeV (the upper limit of the photon tagger during data taking) were generated from a bremsstrahlung spectrum given incident electrons of energy 4.023 GeV (matching the g11 run conditions). We then used the collaboration-standard GEANT-based [30] software suite (GSIM) to model the CLAS acceptance, allowing GEANT to produce the $\Lambda \to p \pi^-$ decay according only to phase space constraints.

We began the data reduction by selecting from the data set all events in which three reconstructed final-state tracks, two of positive charge and one of negative charge, were coincident with a tagged photon. To each event, we assigned the mass hypothesis consistent with K^+, p, and π^- final-state particles, selecting the permutation of positive tracks as that with the value of the invariant mass of the p and π^- candidate tracks, $INV(p, \pi^-)$, closest to the nominal Λ mass. We then applied a loose cut on the square of the total missing mass, MM^2 of each event, keeping events for which $MM^2 \in [-0.002, 0.0005]$ GeV$^2/c^4$.
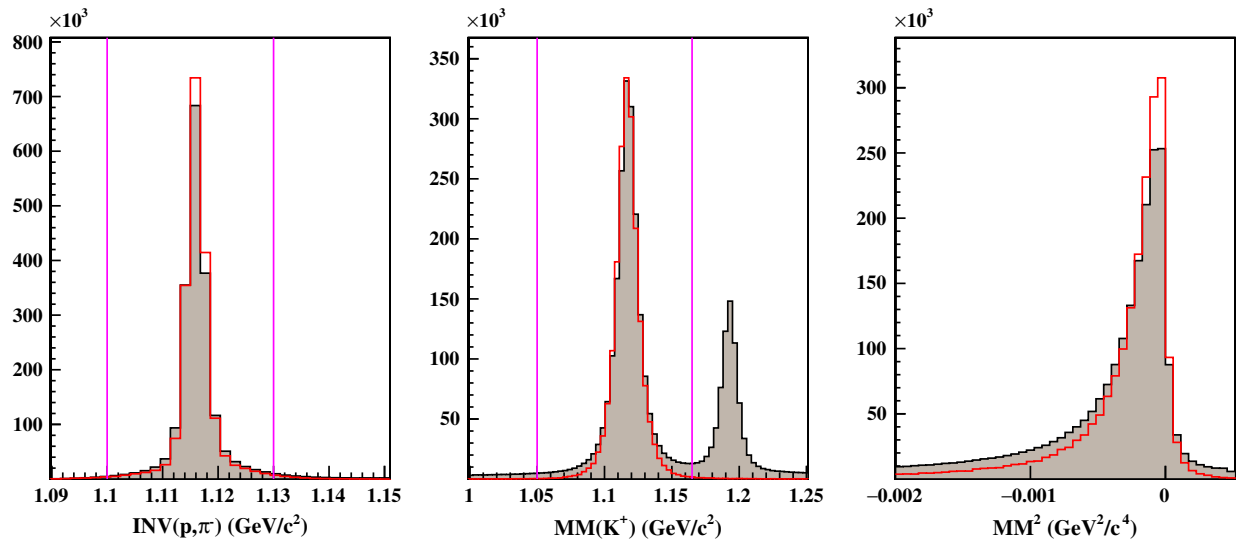

FIG. 2 (color online). $INV(p, \pi^-)$ (left), $MM(K^+)$ (center), and MM^2 (right) distributions for Standard Model data (filled) and MC events (unfilled). In the $INV(p, \pi^-)$ histograms, the distributions are of events that passed all cuts, and the vertical lines show the limits used in signal counting. In the $MM(K^+)$ histograms, the distributions are of events that passed all but the cut on $MM(K^+)$ (thus, the Σ^0 peak is still visible in the data); the vertical lines show the limits of the cut on $MM(K^+)$. In the MM^2 histograms, the distributions are of events that passed all cuts.

To the hypothetical K^+ track, we applied a PID cut based on timing and momentum information from CLAS. CLAS measures the time of flight, tof_m, i.e., the time elapsed between the primary event vertex and the track's triggering of the TOF scintillators. We also calculated a hypothetical time of flight, tof_h, based on our mass hypothesis and tracking information,

$$tof_h = \frac{d}{\beta c} = \frac{d}{c}\left[1 + \frac{m_h^2 c^2}{p^2}\right]^{\frac{1}{2}}, \quad (1)$$

where p is the track's momentum (determined by its curvature through the magnetic field of CLAS), β is related to the track's velocity (determined from tracking and timing information), $\beta = v/c$, m_h is the hypothetical mass for the track (493.7 MeV/c^2 for the K^+), d is the path length of the track from the vertex to the TOF system, and c is the speed of light. This PID cut (and later cuts) is based on the difference of these two quantities,

$$\Delta tof = tof_h - tof_m. \quad (2)$$

In the case where the mass hypothesis is correct, we expect the measured and hypothetical tof to be roughly identical (modulo timing resolution), and thus $\Delta tof \approx 0$. If the hypothetical mass is greater (less) than the particle's actual mass, then we expect the Δtof to be greater (less) than zero. We found that a suitable separation of K^+ candidate tracks from non-K^+ tracks was achieved by a two-dimensional cut, keeping events for which

$$|\Delta tof| \leq (1.8 \text{ ns}) \exp\left(-\frac{p}{1 \text{ GeV}/c}\right) + 0.15 \text{ ns.} \quad (3)$$

The Δtof vs $|\vec{p}|$ plane for signal Monte Carlo events is shown in Fig. 1.

We then made a further cut on the missing mass off of the K^+,

$$MM(K^+) \equiv (p_\gamma + p_t - p_K)^2, \quad (4)$$

where p_γ, p_t, and p_K are the 4-momenta of the incident photon, target proton, and recoil K^+, respectively. We kept events for which $MM(K^+)$ was in the range [1.05 GeV, 1.165 GeV]. In addition to nonstrange backgrounds, this cut removed contamination from photoproduction of higher-mass hyperons that include Λ in their decay chain (predominantly $\gamma p \to K^+\Sigma^0 \to K^+\gamma\Lambda$). We also applied geometrical fiducial cuts, omitting events from regions of the detector for which our simulation is inaccurate. After all cuts, we found that data and MC distributions were quite similar, as shown in Fig. 2.

After these cuts, we identified the signal events by inspecting a histogram of $INV(p, \pi^-)$. Figure 3 shows that this distribution is exceptionally clean. We modeled

these data with a third-order polynomial for background processes and a double Gaussian for signal processes. We then extracted the number of signal events by taking the excess of the data histogram above the background function in all of the histogram bins within 0.015 GeV/c^2 of the nominal Λ mass, yielding $N_{\text{rec}} = 1.861 \times 10^6$ reconstructed $\Lambda \to p\pi^-$ signal events. Because the shape and magnitude of the background and the magnitude of the signal are dependent on kinematics, we vetted the above estimate by separating the data into ten bins in $\cos\theta_{cm}^K$ and performing the fit in each bin. This method again yielded an estimate of $N_{\text{rec}} = 1.861 \times 10^6$.
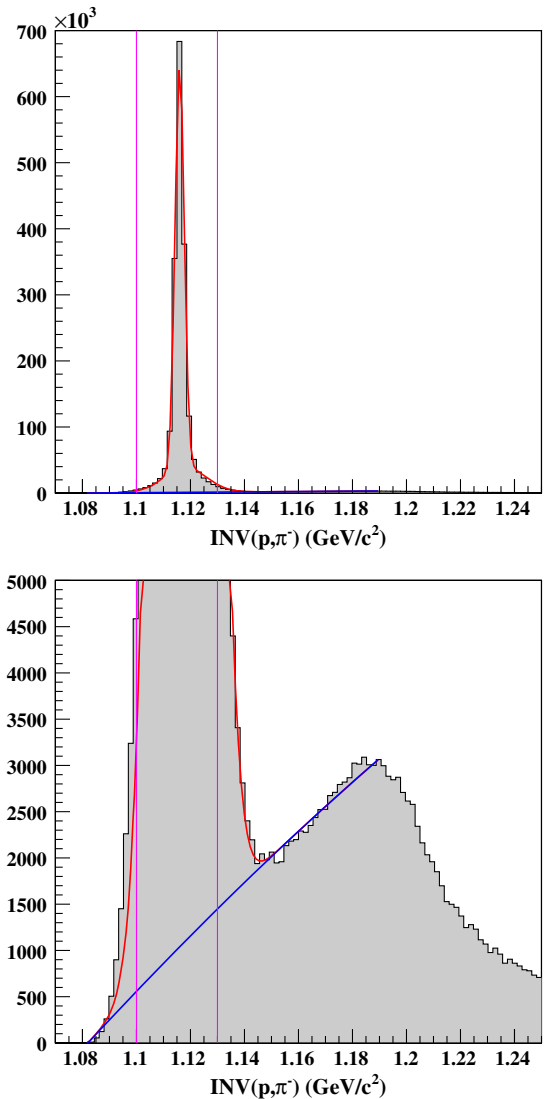

FIG. 3 (color online). Fit to the $INV(p, \pi^-)$ distributions for all events passing the Standard Model decay identification cuts. The lower plot shows the same distribution as the upper, but with a limited vertical scale. The red curve shows the full (signal and background) fit function; the blue curve shows only the polynomial background. The magenta lines show the limits of integration for the event count.

A. Acceptance correction

With the number of reconstructed $\gamma p \to K^+ \Lambda \to K^+ p \pi^-$ events in hand, we could then correct for the effects of the detector's acceptance and the efficiency of our analysis cuts to estimate N_{prod}. We began by applying the cuts described above to the Standard Model MC. Because the generation of MC events matched the data in photon energy distribution and kinematics, we separated the data and MC coarsely into ten bins in $\cos\theta^K_{cm}$. In each bin, we calculated the acceptance $\epsilon_{p\pi^-}(\cos\theta^K_{cm})$ by simply dividing the number of MC events that passed CLAS simulation and acceptance cuts by the total number of MC events generated. We used this factor to determine the number of $K^+ \Lambda \to K^+ p \pi^-$ events produced during the run in each $\cos\theta^K_{cm}$ bin and completed the calculation by summing over the angular bins:

$$N_{\text{prod}} = \sum_{\cos\theta^K_{cm}} \frac{N_{\text{rec}}(\cos\theta^K_{cm})}{\epsilon_{p\pi^-}(\cos\theta^K_{cm})} \qquad (5)$$

$$= 3.71 \times 10^7. \qquad (6)$$

IV. BNV CANDIDATE SELECTION AND OPTIMIZATION

Because of the sensitive nature of the possibility of BNV discovery, we pursued a *blind analysis*. For each of the BNV $\Lambda \to AB$ decay modes under investigation (see Table I), we tuned a set of cuts, C, using the kinematic quantities $MM(K^+)$, $INV(A, B)$, and MM^2, as well as the timing information for A and B. As before with the Standard Model Λ decay, we identified the BNV signal using the $INV(A, B)$ spectrum (except for the $\Lambda \to K^0_s \nu$ channel described below). In tuning each set of cuts, we tried to strike a balance between reducing the large number of nonsignal events and maintaining acceptance for a potentially small BNV signal.

Punzi [31] has proposed a figure of merit for performing such optimizations, which has been used in several other searches for rare reactions. For a set of cuts C, the Punzi figure of merit, $\mathcal{P}(C)$, is defined as

$$\mathcal{P}(C) = \frac{\epsilon(C)}{b^2 + 2a\sqrt{B(C)} + b\sqrt{b^2 + 4a\sqrt{B(C)} + 4B(C)}}, \qquad (7)$$

where $\epsilon(C)$ is the efficiency of the cuts when applied to signal, $B(C)$ is the number of background events passing cuts C, and a and b are the number of standard deviations corresponding to the analysis-defined significance and statistical power. In this analysis, we chose $b = a = 4$, indicating a 4σ confidence level. With these choices, the figure of merit simplifies to

$$\mathcal{P}(C) = \frac{\epsilon(C)}{16(2 + \sqrt{B(C)})}. \qquad (8)$$

We tuned our cuts by simultaneously assessing $\epsilon(C)$ using MC BNV events and $B(C)$ from sidebands of the blinded signal region. In all plots that would identify any BNV signal [e.g., $INV(A, B)$], we blinded the signal region. We postponed the unblinding of the signal regions of all of our data plots until after the optimization of the analysis cuts, once we were confident that all cuts and systematic effects were understood.

For each BNV $\Lambda \to AB$ decay under investigation, we generated 10^6 $\gamma p \to K^+ \Lambda \to K^+ AB$ Monte Carlo events, matching photon energies to the run conditions and $K^+ \Lambda$ kinematics to the measured $d\sigma/d\cos\theta$ (as for the Standard Model MC). We generate kinematics for the $\Lambda \to AB$ decays according only to phase-space constraints. In the case of the $\Lambda \to K^0_s \nu$ reaction, the subsequent $K^0_s \to \pi\pi$ decay was modeled by GEANT at the time of detector simulation.

For each channel, we chose the positive track mass hypothesis that yields a value of $INV(A, B)$ nearest to the nominal Λ mass (as was done for the Standard Model analysis above). The analysis cuts for each channel began with a PID cut on Δtof [see Eq. (2)] for each final-state particle. For each particle type, we applied a loose two-sided cut in the Δtof vs p plane, similar to that applied to the K^+ track for the SM decay. CLAS resolution allowed us to make these cuts loose; however, the characteristic decay length of $K^\pm$ is on the same order as the dimensions of CLAS, and the nontrivial fraction of $K^\pm$ that decay in the detector resulted in these cuts reducing the data sample by approximately half (depending on the number of charged kaons detected for each channel).

A. Example: $\Lambda \to \pi^+ \mu^-$

Here, we demonstrate this process with the $\Lambda \to \pi^+ \mu^-$ channel; other channels, with the exception of the $K^0_s \nu$ decay, were analyzed using the same observables.

For the three charged tracks in each event, we first decided which positive tracks correspond to the recoil K^+ and π^+. We made this assignment by calculating the invariant mass of each positive-negative track pair and choosing the assignment that gave a value nearest the nominal Λ mass. We then applied PID cuts based on the Δtof method to each of the three particles, the boundaries of which are shown in Fig. 4. These cuts are loose, and we have found that their efficiencies for each particle type are similar when applied to broader MC and data samples.

After the PID cuts were made, we turned to analysis cuts based on kinematic observables. For the $\Lambda \to \pi^+ \mu^-$ channel, we made a symmetric cut on MM^2 (centered about 0 with width w_1) and $MM(K^+_r)$ (centered about 1.1186 GeV/c^2, with width w_2). To find the widths, w_1 and
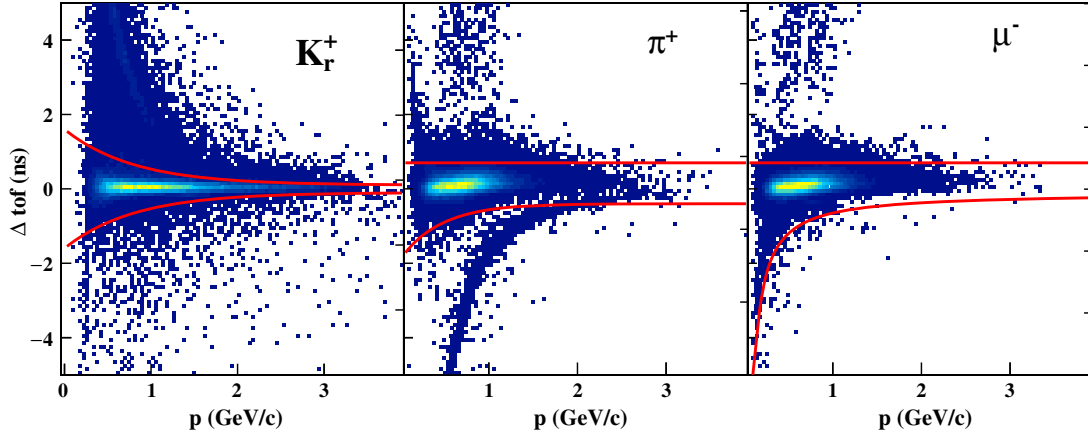
FIG. 4 (color online). Δtof vs p for $\Lambda \to \pi^+\mu^-$ Monte Carlo. The red curves define the boundaries of the PID cuts for each particle type. Shown are the recoil K^+ (left), decay π^+ (center), and decay μ^- (right). The bands with $\Delta tof > 1.0$ ns in the kaon plot represent μ^+ from kaon decays.

w_2, which optimize the Punzi metric, we uniformly sampled 40 values for each width, resulting in 1600 distinct pairs with

$$w_1 \in [0, 0.001] \text{ GeV}^2/c^4 \tag{9}$$

$$w_2 \in [0, 0.03] \text{ GeV}/c^2. \tag{10}$$

We applied these cuts to both signal MC and data and inspected the resulting $INV(\pi^+, \mu^-)$ histograms with the signal region of the data histogram blinded. We defined the signal region to be values of $INV(\pi^+, \mu^-)$ within 0.03 GeV$/c^2$ of the nominal Λ mass (i.e., $[1.086, 1.146]$ GeV$/c^2$) and the sideband regions to be within 0.15 GeV$/c^2$ of the peak (excluding the signal region).

We then used the signal MC distributions before and after cuts to determine the signal efficiency, $\epsilon(C)$. We applied a simple sideband technique to the data $INV(\pi^+, \mu^-)$ histogram to extrapolate $B(C)$, the expected number of background events in the blinded signal region. We then used these values to calculate $\mathcal{P}$ for each width pair (see Fig. 5) and selected the width pair that maximizes $\mathcal{P}$ as optimal. For the $\Lambda \to \pi^+\mu^-$ channel, we found the optimal widths to be $w_1 = 3.25 \times 10^{-4}$ GeV$^2/c^4$ and $w_2 = 9.00 \times 10^{-3}$ GeV$/c^2$. The plots in Fig. 5 illustrate the resulting cuts and the blinded signal plot for this channel.

Figure 5 demonstrates that the optimal cut scheme for this channel is quite restrictive; only five data events populate the (blinded) $INV(\pi^+, \mu^-)$ histogram, and none of these falls within the sideband regions. We thus estimated the expected number of background events in the signal region to be zero. By studying the signal MC for this channel, we estimated that the efficiency of these cuts, $\epsilon(C)$, is 7.91% (including the effects of detector acceptance). The effects of detector acceptance and analysis cuts are similar for all of the charged decay channels. Table II lists the properties of the optimal cuts for each channel.

B. $\Lambda \to \bar{p}\pi^+$

Our analysis of the $\Lambda \to \bar{p}\pi^+$ channel proceeded nearly identically to that of the charged $\Lambda \to m\ell$ channels. We first assigned the positively charged track mass hypothesis by comparing $INV(\bar{p}, \pi^+)$ for the two possible track permutations. We then applied a PID cut in the Δtof vs momentum plane for each particle. Threshold $\bar{p}$ photoproduction via the process $\gamma p \to p p \bar{p}$ occurs at a photon energy of 3.751 GeV; the maximum tagged photon energy in our data set is 3.86 GeV. Unlike in the other charged decay channels where there are significant numbers of each particle type present in the data, the null hypothesis suggests that there should be relatively few antiprotons in the data set. As a result, we used a less restrictive PID cut for the antiproton, keeping events with Δtof between -1.8 and 1.0 ns. Because of the absence of background reactions that produce $\bar{p}$, this PID cut was the most stringent requirement in this channel. We optimized cuts on the MM^2 and $MM(K^+)$ observables using the same method as for the $\Lambda \to m\ell$ channels, yielding optimal cut widths of $w_1 = 5.00 \times 10^{-4}$ GeV$^2/c^4$ and $w_2 = 4.25 \times 10^{-2}$ GeV$/c^2$, respectively, and a signal efficiency of $\epsilon = 4.98\%$.

C. $\Lambda \to K_S^0 \nu$

In addition to the charged decay modes, we searched for the decay of $\Lambda \to K_S^0 \nu$, using the dominant charged decay mode $K_S^0 \to \pi^+\pi^-$. (Observation of the $K^0 \to 2\pi$ selects K_S^0 rather than K_L^0.) Because of this reaction's final-state neutrino, we do not have access to $INV(K_S^0, \nu)$; thus, the analysis described for the charged decay modes is not appropriate for this channel. In addition, the unmeasured momentum of the ν limited our analysis constraints, and we expected more background to pass the optimized cuts.

We began the background separation process by applying two-dimensional PID cuts based on Δtof and momentum to the charged final-state particles (recoil K^+ and the
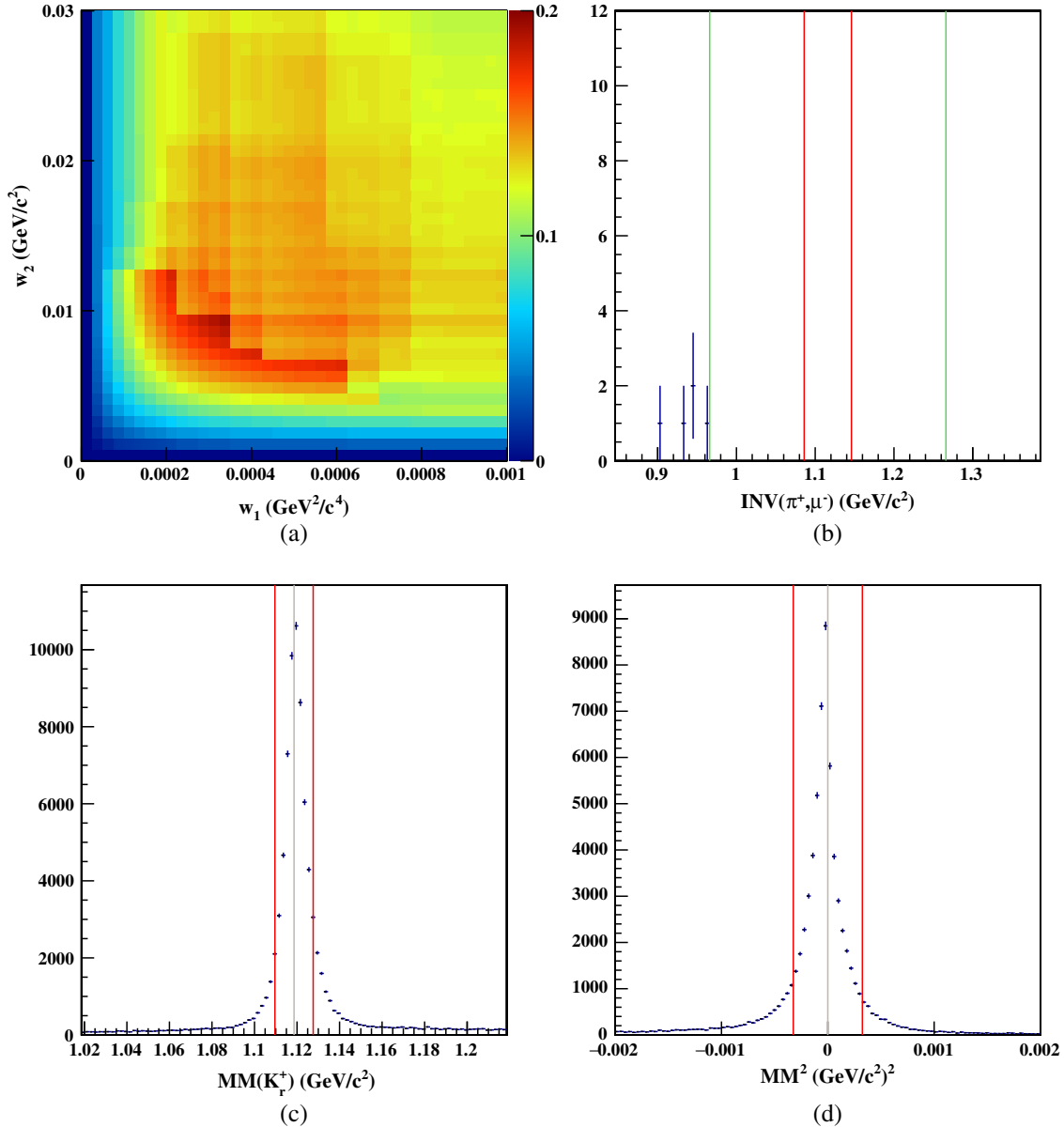
FIG. 5 (color online).   Plots of $\mathcal{P}$ vs cut widths w_1 (GeV$^2/c^4$) and w_2 (GeV/c^2) (a), data $INV(\pi^+\mu^-)$ (b), Monte Carlo $MM(K^+)$ (c), and Monte Carlo MM^2 (d) for the $\Lambda \rightarrow \pi^+\mu^-$ channel. In (b), the vertical red lines show the boundaries of the blinded signal region, and the green vertical lines show the boundaries of the sideband regions. In (c) and (d), the gray and red lines show the center and boundaries of the optimal cuts, respectively.

$\pi^\pm$ from K^0 decay) similar to those for the $\Lambda \rightarrow \pi^+\mu^-$ channel (see Fig. 4). We then optimized a two-dimensional cut motivated by the particulars of this decay. The first is a symmetric cut on MM^2, centered at 0 (the mass of the ν is negligible) with width w_1.

The second cut identifies $\pi^\pm$ pairs that are produced from K^0 decay by inspecting the $\pi^\pm$ opening angle, (θ_o^π), in the c.m. frame,

$$\theta_o^\pi = \cos^{-1}\left(\frac{\vec{p}_+ \cdot \vec{p}_-}{|\vec{p}_+||\vec{p}_-|}\right), \tag{11}$$

where $\vec{p}_\pm$ are the momenta of the decay pions indexed by charge. Due to the breakup energy associated with the $K^0 \rightarrow \pi^+\pi^-$ decay, θ_o^π is constrained to a narrow range for a given value of K^0 momentum. However, for $\pi^+\pi^-$ pairs that do not come from K^0 decay, we expected only the constraints associated with momentum conservation for the entire event, i.e., much less correlation between the pion momenta. Distributions of θ_o^π vs magnitude of K^0 momentum, p_K, for data and signal MC are shown in Fig. 6. We separated $K^0 \rightarrow \pi^+\pi^-$ events by making a two-dimensional cut on θ_o^π vs p_K. To obtain a description of the correlation between θ_o^π and p_K, we fit the two-dimensional histogram

TABLE II.   Inputs to and final calculations for the upper limits on the branching fractions. w_1 and w_2 are the optimized cut widths for each channel. For the charged decay modes, w_1 and w_2 are the widths of the cuts on MM^2 (in GeV^2/c^4) and $MM(K^+)$ (in GeV/c^2), respectively. For $\Lambda \to K_S^0 \nu$, w_1 and w_2 are the widths of the cuts on MM^2 (in GeV^2/c^4) and $K_S^0 \to \pi^+\pi^-$ opening angle, respectively. ϵ is the efficiency for each reaction, calculated using Monte Carlo studies described in the text; N_{eb} is the number of expected background events, calculated from sideband studies and confirmed with Monte Carlo studies; N_{obs} is the number of observed events in the data; N_{UL} is an upper limit on the number of signal events in the data, calculated using the Feldman–Cousins technique [27] for the charged decay modes and likelihood scanning technique for the $\Lambda \to K_S^0 \nu$ channel; and $\mathcal{B}_{UL}$ is the upper limit on the Λ branching fraction for each decay mode.

Reaction	w_1	w_2	ϵ (%)	N_{eb}	N_{obs}	N_{UL}	$\mathcal{B}_{UL}$
$\Lambda \to K^+ e^-$	2.50×10^{-4}	0.01625	4.13	0	1	4.36	2×10^{-6}
$\Lambda \to K^+ \mu^-$	3.25×10^{-4}	0.0125	4.42	0	2	5.91	3×10^{-6}
$\Lambda \to K^- e^+$	1.80×10^{-3}	0.01375	4.63	0	1	4.36	2×10^{-6}
$\Lambda \to K^- \mu^+$	3.00×10^{-4}	0.0300	4.40	0	2	5.91	3×10^{-6}
$\Lambda \to \pi^+ e^-$	2.75×10^{-4}	0.00900	7.02	0	0	2.44	6×10^{-7}
$\Lambda \to \pi^+ \mu^-$	3.25×10^{-4}	0.00900	7.91	0	0	2.44	6×10^{-7}
$\Lambda \to \pi^- e^+$	4.75×10^{-4}	0.0125	8.65	0.75	0	1.94	4×10^{-7}
$\Lambda \to \pi^- \mu^+$	3.50×10^{-4}	0.00900	7.92	0.25	0	2.44	6×10^{-7}
$\Lambda \to \bar{p}\pi^+$	5.00×10^{-4}	0.0425	4.98	0	0	2.44	9×10^{-7}
$\Lambda \to K_S^0 \nu$	0.01875	0.0600	2.23	239.25	-3.88	14.1	2×10^{-5}

of the two observables and found adequate description with the function

$$f(p_K) = 0.319 - \frac{0.459}{p_K + 0.5} + \frac{2.23}{(p_K + 0.5)^2} - \frac{0.641}{(p_K + 0.5)^3}. \tag{12}$$

The cut width, w_2, is implemented by keeping events for which

$$(1 - w_2)f(p_K) \le \theta_o^\pi \le (1 + w_2)f(p_K). \tag{13}$$

The optimization process tested 1600 pairings of cut widths with $w_1 \in [0, 0.15]$ GeV^2/c^4 and $w_2 \in [0, 0.2]$.

Because $INV(K^0, \nu)$ was not accessible, we used the $MM(K^+)$ distributions to estimate $\epsilon(C)$ and $B(C)$, and ultimately to identify the signal. We chose the blinded signal region to be within 0.03 GeV/c^2 of the Λ mass peak in the $MM(K^+)$ spectrum determined from Standard Model data and MC, 1.186 GeV/c^2, and the sideband regions to be within 0.15 GeV/c^2 of the peak (excluding the signal region). We found the optimal widths to be $w_1 = 1.875 \times 10^{-2}$ GeV^2/c^4 and $w_2 = 0.0600$, yielding an efficiency of 2.23% and 239.25 estimated background events in the signal region. The $MM(K^+)$ distribution for data events after unblinding is shown in Fig. 7.
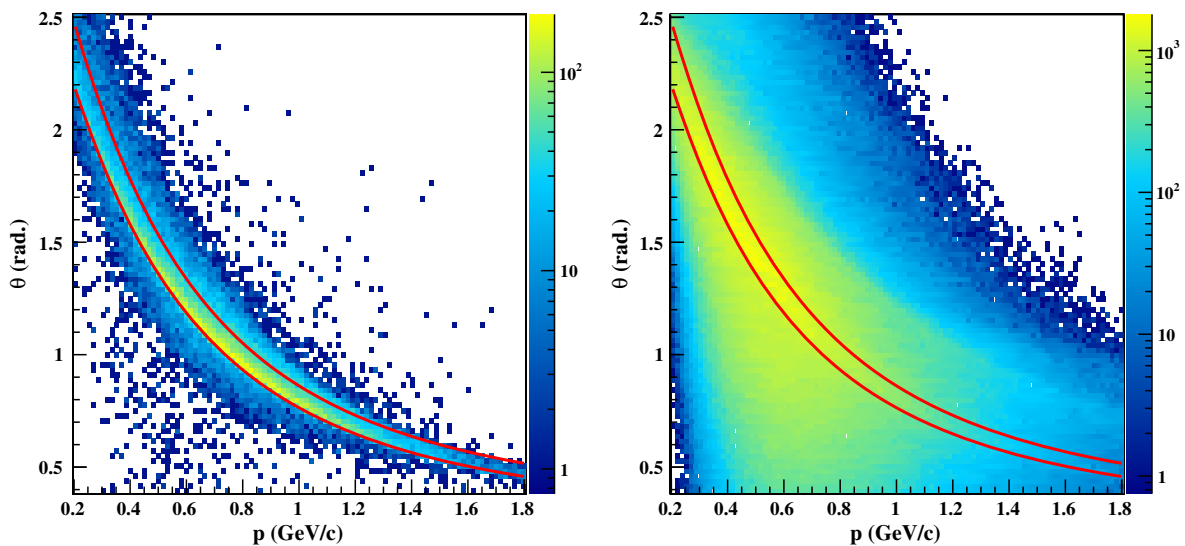

FIG. 6 (color online). $K_S^0 \to \pi^+\pi^-$ opening angle vs p for $\Lambda \to K_S^0 \nu$ Monte Carlo (left) and data (right) after PID cuts. The red curves demonstrate the boundaries of the optimized cut.
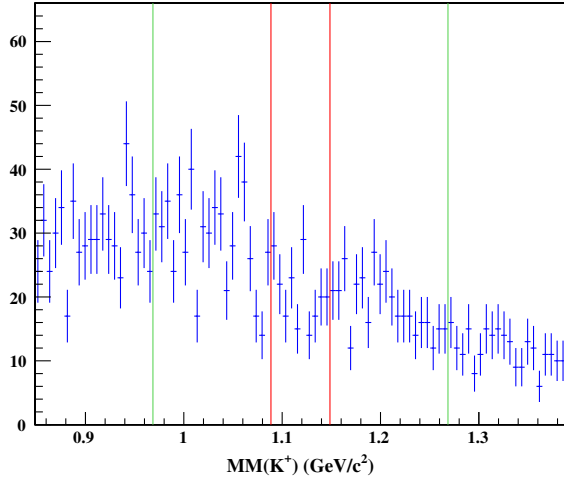
FIG. 7 (color online). Unblinded $MM(K^+)$ distribution for data events after the application of cuts optimized for the $\Lambda \to K_S^0 \nu$ channel. The red vertical lines show the boundaries of the blinded signal region, and the green vertical lines show the boundaries of the sideband regions.

D. Assessing background signatures

Because of the sensitive nature of a positive signal identification, understanding the signature (shape) of the background in signal identification histograms is crucial. If a peak is present when the data is unblinded, we must be sure that the peak represents the BNV signal and is not merely an unfortunate distortion of the background events due to the cuts used. To assess the signature of the background events in $INV(A, B)$ and $MM(K^+)$ distributions, we generated 5×10^5 Monte Carlo events for each of six background reactions:

   (i) $\gamma p \to K^+ \Lambda \to K^+ p \pi^-$
  (ii) $\gamma p \to K^+ \Sigma^0 \to K^+ p \pi^- \gamma$
 (iii) $\gamma p \to p e^+ e^-$
 (iv) $\gamma p \to p \mu^+ \mu^-$
  (v) $\gamma p \to p \pi^+ \pi^-$
 (vi) $\gamma p \to p K^+ K^-$
(vii) $\gamma p \to p \pi^+ \pi^- \pi^0$

These reactions were chosen either for their abundance in the data set (combination of a large cross section and detectability in CLAS) or for their similarity to the BNV channels investigated (similar final-state particles). After applying the optimized cuts for each BNV channel to these MC events, we found that very few events pass the cuts; no channel's cuts allow more than one background MC event into the signal region of the $INV(A, B)$ or $MM(K^+)$ histograms. Thus, we claim that none of the background reactions investigated create an excess in the signal regions.

V. RESULTS

A. Charged decays

After the selection criteria were finalized using the Monte Carlo and sideband studies, we applied these cuts

to the unblinded data. For the nine decay modes where the final state could be completely reconstructed, we found the number of observed events in the signal region, N_{obs}, to be between 0 and 2, consistent with background estimates from the cut optimization studies. For these decay modes, we used the Feldman–Cousins approach [27] to determine upper limits on the reconstructed signal yields, N_{UL}.

The Feldman–Cousins approach provides a way to estimate upper confidence limits for null results. The inputs are the expected number of background events (N_{eb}) and the observed number of events (N_{obs}). We estimated the expected number of background events from the sidebands in the data (see the previous section). N_{obs} and N_{eb} values for each decay mode are shown in Table II. Fractional numbers are given when only one event was observed in a sideband region that spans a greater range than the signal region.

These provided the input to the Feldman–Cousins method, and we quote the upper limit on the reconstructed signal yield at 90% confidence level (N_{UL}), shown in Table II. To calculate the upper limit on the branching fraction ($\mathcal{B}_{\mathrm{UL}}$), we used the efficiency (ϵ) for each decay mode as determined from Monte Carlo studies and the total number of $\gamma p \to K^+ \Lambda \to K^+ p \pi^-$ events produced during the data-taking period, N_{prod} [see Eq. (6)],

$$\mathcal{B}_{\mathrm{UL}} = \mathcal{B}_{p\pi} \frac{N_{\mathrm{UL}}}{\epsilon N_{\mathrm{prod}}}, \tag{14}$$

where $\mathcal{B}_{p\pi} = 0.639 \pm 0.005$ is the $\Lambda \to p\pi^-$ branching fraction [12]. The $\mathcal{B}_{\mathrm{UL}}$ values for all charged decay modes are shown in Table II.

B. $\Lambda \to K_S^0 \nu$

For the $K_S^0 \nu$ decay mode, a BNV signal would manifest itself as a peak in the $MM(K^+)$ distribution at the Λ mass. When we unblinded the $MM(K^+)$ histogram, we observed no such peak and found a number of events in the signal region that is consistent with the background study above. The number of events in the signal region was much larger than is normally handled by the Feldman–Cousins approach; thus, we perform a likelihood scan to determine the upper limit on N_{UL}.

We performed an unbinned maximum likelihood fit to the data in this region using an exponential probability density function (PDF) to describe the background and a sum of two Gaussians to describe the signal. The shape of the background was allowed to vary in the fit, as are the numbers of signal and background events. The parameters describing the Gaussians (i.e., means and widths) were fixed to values determined from Monte Carlo studies.

The fit converged to a central value of $N_{\mathrm{obs}} = -3.88 \pm 8.9$ signal events, consistent with zero signal events. To check whether or not this negative value is of concern, we sampled from a distribution described by the background

parameters returned by the fit to generate 1000 mock "background-only" samples and fit them to a background-plus-signal hypothesis. About 50% of these fits returned a negative value for the signal, and about 35% returned a value more negative than what was found in the data. We determined that the negative value is an artifact of fitting to a small number of points using a function with as much freedom as we use. We note that nowhere does the total PDF go negative.

To calculate an upper limit on the signal yield, we scanned the likelihood function by performing a series of fits where the signal yield (N) is varied around the best fit value N_{obs} and the other parameters were refit to map out the difference in the ln-likelihood: $\Delta \ln \mathcal{L} = \ln \mathcal{L}(N_{\mathrm{obs}}) - \ln \mathcal{L}(N)$. We integrated the function $y = e^{-\Delta \ln \mathcal{L}}$ over N. We ignored the unphysical region with $N < 0$ and calculated the integral for $N > 0$. We noted the value of N which encloses 90% of the area above $N = 0$ and interpreted this as the upper limit on the signal yield returned by the fit at 90% confidence level. This procedure returned an upper limit (N_{UL}) of 14.1 signal events.

C. Experimental uncertainties

Uncertainty in $\mathcal{B}_{\mathrm{UL}}$ comes from the world average of the $\Lambda \to p\pi^+$ branching fraction (0.8%) [12] and statistical and systematic uncertainties from the extraction of N_{prod} and cut efficiencies for each BNV channel. We found a 6.1% relative uncertainty in N_{prod} by combining the 0.02% systematic uncertainty due to the $INV(p, \pi^-)$ peak fitting procedure, the $\approx 6\%$ systematic uncertainty in CLAS acceptance calculation (taken from previous hyperon production analysis [29]), and the 0.64% statistical uncertainty in $\epsilon_{p\pi^-}$ (estimated with binomial statistics). We estimated the uncertainty in ϵ for each BNV channel by comparing the effects of optimized $MM(K^+)$ and MM^2 cuts on MC and Standard Model data distributions and found it to be $\approx 7.6\%$. We combined all uncertainties in quadrature to find a relative uncertainty in $\mathcal{B}_{\mathrm{UL}}$ of $\approx 9.8\%$. With this estimate

of the combined uncertainty in hand, we quote the final $\mathcal{B}_{\mathrm{UL}}$ results to one significant figure (see Table II).

VI. SUMMARY

The analysis described here represents the first search for baryon and lepton number violating decays of the Λ hyperon. Though similar studies have been performed with much higher sensitivities for decays of the nucleon, this study offers the first direct probe of BNV processes involving strange quarks in the initial state. Using a data set for photoproduction off of the proton collected with the CLAS detector at Jefferson Laboratory containing roughly 1.8×10^6 reconstructed $\gamma p \to K^+\Lambda \to K^+ p\pi^-$ events, we have searched via blinded analysis for BNV decays of the Λ to either meson-lepton pairs or to $\bar{p}\pi^+$. We found no BNV signal in any of the ten decay channels investigated and set upper limits on the branching fraction for each of the processes studied in the range 7×10^{-7} to 2×10^{-5}.

[1] S. Glashow, Nucl. Phys. **22**, 579 (1961).

[2] S. Weinberg, Phys. Rev. Lett. **19**, 1264 (1967).

[3] A. Salam, Conf. Proc. **C680519**, 367 (1968).

[4] P. Coppi, How Do We Know Antimatter Is Absent?, eConf C040802, L017 (2004).

[5] G. Steigman, Annu. Rev. Astron. Astrophys. **14**, 339 (1976).

[6] A. Sakharov, Pis'ma Zh. Eksp. Teor. Fiz. **5**, 32 (1967); reprinted in *The Early Universe* (Westview, Boulder, 1994), p. 371; and in *Cosmology and Particle Physics* (American Association of Physics Teachers, College Park, 1991),

p. 106; and in Usp. Fiz. Nauk **161**, 61 (1991)[Sov. Phys. Usp. **34**, 392 (1991)].

[7] V. Kuzmin, V. Rubakov, and M. Shaposhnikov, Phys. Lett. B **155**, 36 (1985).

[8] H. Georgi and S. Glashow, Phys. Rev. Lett. **32**, 438 (1974).

[9] T. Cheng and L. Li, *Gauge Theory of Elementary Particle Physics*, Oxford Science Publications (Clarendon, Oxford, England, 1984).

[10] H. Nishino *et al.* (Super-Kamiokande Collaboration), Phys. Rev. Lett. **102**, 141801 (2009).

[11] K. Abe *et al.* (Super-Kamiokande Collaboration), Phys. Rev. D **90**, 072005 (2014).

[12] K. A. Olive *et al.* (Particle Data Group), Chin. Phys. C **38**, 090001 (2014).

[13] R. Godang *et al.* (CLEO Collaboration), Phys. Rev. D **59**, 091303 (1999).

[14] Y. Miyazaki *et al.* (BELLE Collaboration), Phys. Lett. B **632**, 51 (2006).

[15] R. Aaij *et al.* (LHCb Collaboration), Phys. Lett. B **724**, 36 (2013).

[16] S. Chatrchyan *et al.* (CMS Collaboration), Phys. Lett. B **731**, 173 (2014).

[17] P. del Amo Sanchez *et al.* (*BABAR* Collaboration), Phys. Rev. D **83**, 091101 (2011).

[18] P. Rubin *et al.* (CLEO Collaboration), Phys. Rev. D **79**, 097101 (2009).

[19] G. Abbiendi *et al.* (OPAL Collaboration), Phys. Lett. B **447**, 157 (1999).

[20] W.-S. Hou, M. Nagashima, and A. Soddu, Phys. Rev. D **72**, 095001 (2005).

[21] A. Serebrov *et al.*, Phys. Lett. B **663**, 181 (2008).

[22] K. Abe *et al.* (Super-Kamiokande Collaboration), Phys. Rev. D **91**, 072006 (2015).

[23] K. Babu and R. Mohapatra, Phys. Lett. B **518**, 269 (2001).

[24] B. Dutta, Y. Mimura, and R. N. Mohapatra, Phys. Rev. Lett. **96**, 061801 (2006).

[25] S. Nussinov and R. Shrock, Phys. Rev. Lett. **88**, 171601 (2002).

[26] F. Wilczek and A. Zee, Phys. Rev. Lett. **43**, 1571 (1979).

[27] G. J. Feldman and R. D. Cousins, Phys. Rev. D **57**, 3873 (1998).

[28] B. Mecking *et al.*, Nucl. Instrum. Methods Phys. Res., Sect. A **503**, 513 (2003).

[29] M. E. McCracken *et al.* (CLAS Collaboration), Phys. Rev. C **81**, 025201 (2010).

[30] R. Brun, F. Carminati, and S. Giani, Report No. CERN-W-5013, 1994.

[31] G. Punzi, Sensitivity of Searches for New Signals and Its Optimization, eConf C030908, MODT002 (2003).